ELEVENTH EUROPEAN ROTORCRAFT FORUM

Paper No. 4

MACH NUMBER SCALING OF HELICOPTER ROTOR BLADE/VORTEX INTERACTION NOISE

Kenneth P. Leighton
General Electric Company
Syracuse, New York USA

and

Wesley L. Harris
Massachusetts Institute of Technology
Cambridge, Massachusetts USA

September 10-13, 1985
London, England UK

The City University, London, EC1V OHB, England

MACH NUMBER SCALING OF HELICOPTER ROTOR BLADE/VORTEX INTERACTION NOISE

Kenneth P. Leighton
General Electric Company
Syracuse, New York USA

and

Wesley L. Harris
Massachusetts Institute of Technology
Cambridge, Massachusetts USA

ABSTRACT

An investigation of blade slap due to blade vortex interaction (BVI) has been conducted in the M.I.T. 5 by 7-1/2 foot anechoic wind tunnel. This investigation consisted of an examination of BVI blade slap for two, three, and four-bladed model helicopter rotors at tip Mach numbers ranging from 0.20 to 0.50. The blade slap contour obtained for the two-bladed rotor configuration is used as a baseline to determine the effect of blade number on the BVI blade slap.

A peak blade slap Mach number scaling law has previously been developed for two-bladed rotors for a limited number of test conditions. The BVI blade slap has been shown to obey an M_T^6 law. A comparison of peak blade slap SPL's for three and four-bladed rotor configurations shows very good agreement with the sixth power law for all conditions tested.

In addition to documenting the similarities and differences between configurations, directivity studies of the BVI blade slap were conducted in two separate planes. Although these directivity patterns exhibited differences, they both indicated that the maximum SPL was measured directly beneath the rotor shaft. In all studies the presence of blade slap was determined subjectively by observing the pressure profile on an oscilloscope and listening to the transient acoustics signature.

NOMENCLATURE

a	Speed of sound (ft/sec)
b	Span of rotor blade
B	Number of blades
BVI	Blade/vortex interaction
c	Blade chord (ft)
C_n	Complex Fourier coefficient of sound radiation
M_t	Rotational tip Mach number ($\Omega R/a$)
R	Rotor radius (ft)
r_1	Observer location from rotor disc center
SPL	Sound pressure level--B-weighted (dB)
T	Thrust (lbs)
V_{tun}	Tunnel velocity (ft/sec)
y	Distance along blade span
α_s	Shaft tilt angle (°)
γ	Blade loading harmonic
C_T/σ	Thrust coefficient/rotor solidity $= T/\rho(\Omega R)^2 \pi R^2 \times \pi R/Bc$
ξ	$= \eta/b$ = non-dimensional rotor blade span
η	Blade spanwise coordinate
ϕ	Azimuthal angle
Φ	Function to account for phase difference
λ_{max}	Largest acoustic wavelength of interest
μ	Advance ratio = $V_{tun}/\Omega R$
ρ	Density of air (slugs/ft^3)
θ_T	Collective pitch at tip (°)
Ω	Angular velocity (rad/sec)

1. INTRODUCTION

The helicopter rotor is a major source of the radiated noise. These rotors operate in complex aerodynamic environments. The associated noise which they generate is correspondingly complex. This noise may be divided into two groups: (1) broadband noise and; (2) harmonic noise.

Broadband noise is the sound generated by random loadings due to inflow turbulence, vortex shedding, boundary layers, and possibly stall. Broadband noise is characterized by a continuous but sometimes peaked frequency spectrum.

Harmonic noise is characterized by discrete peaks in the frequency spectrum occuring at integral multiples of the blade passage frequency. The sources of this type of noise are numerous. Steady loads due to the integrated torque and thrust forces produced by the rotor to sustain flight generate rotational noise. Volume-velocity effects due to finite blade thickness, along with shock waves generate impulsive harmonic noise at high rotor blade speeds. Rapid stalling and recovery may also be a source of impulsive noise. And blade/vortex interations occuring over very small azimuths generate rapidly fluctuating forces which may lead to the radiation of impulsive noise. When it does occur, impulsive noise, also known as blade slap has been shown to be the prominent far field acoustic phenomenon. Impulsive noise is a form of harmonic noise.

The rotor blade tip generates a strong vortex which affects the entire flow field of the rotor. As discussed in Reference [1], there is a continuous shedding of vortices along the blade which forms a vortex sheet. The strongest of these occurs at the blade tip. This system exists for each rotor blade, and is distorted by the systems of all other blades in a specific rotor configuration. The vortex sheet outboard of the point of maximum bound vorticity tends to roll up very rapidly into discrete vortex filaments behind the rotor wake. Blade/vortex interaction (BVI) blade slap has been found to occur at those conditions where the tip vortex can be expected to pass very close to the rotor. For a single main rotor these conditions may occur during the autorotative descent, partial power descent, steep turns, and decelerations. For further discussions on the aerodynamics involved in these conditions, as well as low speed forward flight, the reader is directed to the work of Hubbard [2], Crimi [3], and White [4].

The noise from a rotor blade due to a BVI may result from a number of sources. For rotors operating at high rotational Mach numbers, Tangler [5] has shown that a vortex may induce a shock which propagates to the far field as impulsive noise. The additional velocity of the vortex may also contribute compressibility noise. At low and moderate tip speeds ($M_T < 0.6$) where compressibility and shock waves are unlikely to occur, unsteady loads induced by a BVI may generate impulsive noise [6, 7]. Much interest and research has been conducted on BVI blade slap. Charles [8] conducted full-scale tests with airframe mounted microphones to record the near field acoustcs of the helicopter. He developed boundaries which identified the specific flight conditions for the generation of BVI blade slap. Boxwell and Schmitz [9] conducted full-scale test on a number of different rotor types (UH-1H, Ogee tip,

Kaman K747, AH-1S 540) to determine some far field characteristics of the BVI noise phenomena. Model scale studies for both high rotational speed ($M_T > .65$) [10] and low rotational speed ($M_T < .50$) [11] have been reported. Some of these model scale tests have been conducted to demonstrate the relative impulsive noise generation of various tip shapes [12, 13]. Though some of these tips show promise in helping to relieve the BVI blade slap problem, the cost to performance may preclude their use.

The tip Mach number of this parametric investigation does not exceed 0.50. For this reason it is concluded that BVI is the mechanism responsible for blade slap. Previous flow visualization studies further substaintiate this conclusion [14]. A Mach number scaling law for BVI blade slap in this facility has been developed for a 2-bladed rotor configuration [15]. This study attemps to determine the validity of the scaling law for 3 and 4-bladed rotors. Simultaneous thrust, and acoustic time histories are acquired to determine a relationship between the performance of the rotor and the radiated BVI impulsive noise.

2. EXPERIMENTAL EQUIPMENT AND PROCEDURES

2.1 Introduction

A study of the effects of one parameter, with all others unchanged, on a model rotor in various flight conditions may be conducted in an anechoic wind tunnel. A parametric investigation of model helicopter rotor blade slap in simulated descent was performed in the MIT Anechoic Wind Tunnel Facility. Specifically, the effects on the blade slap signal of the following parameters were investigated: advance ratio, blade collective pitch, blade loading (C_T/σ), number of blades, and shaft tilt results. Blade slap contours are developed for interpretation of test results. Blade slap contours illustrate the advance ratio and shaft tilt combination for which BVI blade slap exists. Comparison of contours indicate salient qualitative differences between various blade number configurations. These contours may be used with the (C_T/σ) values provided by the blade slap windows to obtain the pertinent data acquired in these tests.

2.2 The MIT Anechoic Wind Tunnel Facility

This study was done in the MIT Anechoic Wind Tunnel Facility. The tunnel has a 5x7-1/2 foot open jet test section which is enclosed within an acoustically treated working chamber (see Fig. 2.1). The streamwise dimension of the working chamber is 12 feet. Six-inch thick polyurethane open cell foam was used as acoustic treatment for the floor of the chamber. Cremer blocks [16], porous cloth bags filled with fiberglass blocks, cover both ceiling and wall surfaces. This treatment, along with noise reduction techniques employed throughout the remainder of the closed tunnel circuit provide free field conditions (6dB reduction in SPL for a doubling of distance) down to 160 Hz. Maximum airstream Mach number for this facility is 0.10.

2.3 The Model Rotor System

A new drive system was installed for these series of tests. A Denison series 6 hydrostatic transmission system was employed. This consists of a hydraulic pump and motor system capable of developing 204 hp (continuous), at 3000 RPM. By reducing the displacement of the motor through a valve controlled manual over-ride system, overspeed is possible up to 3900 RPM. Details on operating torques, pressures, and other salient characteristics may be found in Abex Denison Bullentin 1107-J. The model numbers for the pump and motor are P7P-2R1A-100-A and M6H-3N1C-2A0-A respectively.

The maximum deliverable horsepower with the currently installed configuration is 100 hp. This is due to the fact that a 100 hp electric motor supplies power to the hydraulic pump. The drive system speed and direction is controlled by regulating the displacement of the hydraulic pump. This is accomplished through the use of a variable speed electric motor. The shaft of the variable speed electric motor is mechanically coupled to the rotary servo stem of the hydraulic pump. The action of the rotary servo stem causes the displacement of the hydraulic pump to vary from zero displacement to full displacement either in the clockwise or counterclockwise directions. The speed and direction of the hydraulic motor immediately follows the changes of the hydraulic pump.

The model rotor consists of a 4.17 foot diameter rotor model of fiberglass which may be mounted on a rotor hub attached to a thrust dynamometer. The airfoil is a NACA 0012 section with 8 degrees of linear washout (-8 degrees twist). The hub, which floats on two sets of four spokes, can accept up to 8 blades. These flexures can be preloaded by means of nuts located at the end of each spoke. Four sets of BLH-SPB- 3-20-35 semiconductor strain gauges are mounted on the flexures. The system was designed to insure that bending and torsional modes and frequencies are higher than the longitudinal natural frequency, thereby negating their effect on the system stability. During operation, the fundamental blade passage frequency is always lower than the natural frequency of the system. This is to guarantee resonance free behavior of the system. Signals are transmitted from the rotating system to the fixed frame via a Lebow slip ring assembly. Further details of the thrust dynamometer as well as its calibration may be obtained from references [17] and [18]. The rotor shaft is capable of tilting forward 20 degrees and backward 10 degrees from the vertical. Specifications of the model rotor system are given in Table 2.1.

For these experiments a torque measurement system was designed and installed. This system consists of a four arm active strain gage bridge mounted on the upper portion of the rotating shaft slightly below the rotor hub assembly. This system results in automatic temperature compensation for all gages and elimination of the effects of all strains other than torsional strains. For full elimination of all non-torsional strains, care must be exercised in mounting the gages at precisely 45° with the shaft axis.

2.4 The Data Acquisition Instrumentation

The data acquired in each experiment in this work consists of four types. They are: acoustic, rotor RPM, rotor thrust, and tunnel velocity.

A schematic of the data acquisition instrumentation is shown in Figure 2.2.

All microphones used were Bruel and Kjaer (B&K) Type 4133, 1/2 inch condenser microphones. They were used in conjunction with a B&K Type 2615 cathode follower. The acoustic signal was directed to either a B&K Type 2604 amplifier or a B&K Type 2107 frequency analyzer (with amplifier circuit). Calibration of the microphone was accomplished using a B&K Type 4220 piston phone at 124 dB and 250 Hz. Also used was B&K Type UA 0385 nose cone for measurements made within the windstream of the open jet test section.

Once a suitable internal weighting network has filtered the acoustic signal, the pressure-time history was sent to an analog and a digital oscilloscope. The digital device was a Nicolet 206 Explorer III, with external disk memory. The analog scope was a Textronix Type 502 dual beam oscilloscope. The analog scope was used to observe acoustic, RPM and thrust capture, digitize and store the transient acoustic signature, as well as a number of one per revolution pulses. The one per revolution triggering pulse was generated by an optical diode device which sensed a notch in a circular plate which rotated at the rotor speed. This pulse, having a period of $2\pi/\Omega$ was measured and displayed using a Data Precision Model 5740 period counter.

Once the real time blade slap signature has been stored on floppy diskette, an HP-7035 X-Y recorded was utilized to plot the pressure-time histories.

The steady rotor thrust was provided by the dynamometer described above. A voltage signal proportional to the deflection of the cantilever beam assembly within the dynamometer assebly was displayed on a digital voltmeter. Static and dynamic load calibrations done before the initiaion of testing provide the corresponding thrust level. A zero reading of the dynamometer is taken at the end of each set of runs. This is to determine the zero shift of the output signal due to heating of the gages during a test run. This signal is then subtracted from the total measured thrust signal value.

Finally, a standard pitot-tube assembly is used to measure wind tunnel velocities. As shown in the data acquisition instrumentation schematic a set of headphones is used to monitor the sound at the microphones during the experiments.

2.5 Data Reduction Procedures

Initially, blade slap studies were conducted to confirm the two-bladed boundaries obtained before modification of the rotor system [7]. These boundaries are used as the baseline data by which the relative effects of additional blades may be evaluated. Once these data were confirmed, methods used previously for generating blade slap contours/boundaries were employed. For generation of the blade slap contours, shaft angle, blade collective pitch angle and rotor RPM are held constant. The advanced ratio is increased from zero by increasing tunnel speed until blade slap was encountered. At this point very small changes are made in advance ratio to determine the condition of maximum, or peak blade slap. Advance ratio was continuously

increased until blade slap was no longer present. This marked the upper boundary of the blade slap contour. This was repeated for increasing shaft angle until a shaft angle was reached where blade slap did not exist for any advance ratio. Utilizing this technique blade slap contours were produced.

The data gathered in this study were in the form of peak to peak B-weighted sound pressure levels of real-time transient noise signals. A one per revolution pulse was used to trigger the oscilloscope traces. This one per revolution pulse may be used to determine the azimuthal angle of the blades during the blade/vortex interaction. This allows one to determine the shift, if any, of this azimuthal angle due to the variation of any other parameter.

It is important to note here that no objective method presently exists to define blade slap. In this study subjective evaluations of the acoustic signal were employed to determine the presence of BVI blade slap. These evaluations consist of visually monitoring the pressure time histories displayed on the oscilloscopes while simultaneously listening to the sound on a set of headphones.

During all of the tests, steady thrust measurements were supplied by the dynamometer. These measuements were used to generate C_T/σ "windows" with collective pitch a parameter. These "windows" were determined during the previously mentioned test phase for two-bladed rotors only. A separate set of conditions was not required for determination of these "windows".

An important phase of the research effort was the determination of a peak blade slap Mach number scaling law. The shaded areas of the blade slap contours represent regions where the overall SPL was within 1 dB of the maximum SPL at that shaft angle. Once the peak slap advance ratio was determined at one RPM, tests were conducted which varied only rotational tip speed. The results of this test phase were then compared to a theoretical prediction scheme to determine the degree of correlation. A scaling law had previously been determined for certain two-bladed rotor conditions [15].

Finally, directivity patterns of the blade slap noise were measured. These patterns of the blade slap profile at various observed angles proved useful in identifying and characterizing the blade slap producing mechanisms.

Two types of directivity patterns were acquired. The first type was made in a vertical plane normal to the tunnel wind axis as indicated in Fig. 2.1. The directivity patterns were measured at a constant radial distance of 48 inches from the rotor hub position at zero shaft tilt angle. Because of the inverted operation of the rotor, the directivity pattern corresponds to being below the rotor plane of an actual helicopter in flight. The second type of directivity pattern is acquired in a vertical plane parellel with the tunnel wind axis and normal to the first type of directivity pattern. The microphone is kept at a constant azimuthal angle (180°), while the angle the radius vector makes with the horizontal varies from 90° to 25°. This corresponds to angles moving from directly below the rotor (90°) to a position in a forward quadrant of the rotor (upstream).

The test range of tip Mach number for these experiments is 0.20 through 0.50. This corresponds to a Reynolds number range of 2.39×10^5 through 6.34×10^5. This is a Reynolds number based on the chord of the blades and the advancing tip speed.

3. Mach Number Scaling Law

Lowson and Ollerhead [19] derived the expressions for the far field acoustic radiation due to a rotating fluctuating point force. The complex Fourier coefficient C_n of sound radiation from a source at a distance r_1 from axis of rotation, with suitable simplification is shown to be [20]

$$C_n = \sum_{\gamma=0}^{\infty} (i)^{-(n-\gamma)} \frac{n\Omega X}{4\Pi a r_1^2} [i a_{\gamma T} - b_{\gamma T}] \; J_{n-\gamma}(nMy/r_1). \tag{1}$$

This holds everywhere except in or near the plane of the rotor, where the lift forces are essentially zero, and drag and centrifugal forces dominate the acoustic field.

For the case of a helicopter rotor, the observed sound is the result of the continuous distributed loading along the blade span. Therefore, the power spectral density of radiated sound $P(X,n)$ at an observer location X is given by

$$P(X,n) = \lim_{T\to\infty} \frac{1}{T} \int_0^T dt \iint_{\eta\eta} C_n(X,\eta) C_n^*(X,\eta') d\eta d\eta' \tag{2}$$

where C_n^* is the complex conjugate of C_n. After non-dimensionalizing the span and combining terms the power spectral density becomes

$$P(X,\eta) = \frac{1}{4\Pi} \left[\frac{n\Omega X}{a\, r_1^2}\right]^2 \left[\frac{1}{2} \rho o b^2 \Omega^2 C\right]^2 b^2$$

$$x \sum_{\gamma=0}^{\infty} \sum_{\gamma=0}^{\infty} \int_0^1 \int_0^1 C_{\gamma T} \; C_{\gamma' T} \; \xi^2 \xi_{1e}^2 \; i[\phi\gamma - \phi\gamma']$$

$$x \; J_{n-\gamma}(nM_t y/r_1 \xi) \; J_{n-\gamma 1}(nM_t y/r_1 \xi_1) d\xi d\xi_1 \tag{3}$$

For geometrically similar blades, the quantities inside the summation sign remain unchanged provided that $[M_t(y/r_1)]_1 = [M_t(y/r_1)]_2$. Hence the Mach number scaling law reduces to

$$P(X_2,n,M_{t_2}) = P(X_1,n,M_{t_1}) \left[\frac{M_{t_2}}{M_{t_1}}\right] \left[\frac{C_2}{C_1}\right] \left[\frac{r_1}{r_2}\right]^2 \left[\frac{\sin\gamma_2}{\sin\gamma_1}\right]^2 \tag{4}$$

where $\sin\gamma = x/r_1$

In the case of forward flight, r_1 should be replaced by $r_1 (1-M_{or})$, where M_{or} is the component of forward flight Mach number in the direction of the observer. So for forward flight the Mach number scaling formula becomes

$$P(X_2,n,M_{t_2}) = P(X_1,n,M_{t_1}) \left[\frac{M_{t_2}}{M_{t_1}}\right]^6 \left[\frac{C_2}{C_1}\right]^2 \left[\frac{r_1}{r_2}\right]^2 \left[\frac{\sin\alpha_2}{\sin\alpha_1}\right]^2$$

$$\times \frac{1 + \mu_1 M_{t_1}\cos\alpha_1\cos\alpha_1}{1 + \mu_2 M_{t_2}\cos\alpha_2\cos\alpha_2} \quad . \tag{5}$$

A special case arises when the observer location is above the axis of the rotor. In this case, $y/r_1 = 0$, and hence the only term in expression (1) contributing to the entire sound field will be that with $n=\gamma$. Hence, both expression (4) and (5) reduce to

$$P(X_2,n,M_{t_2}) = P(X_1,n,M_{t_1}) \left[\frac{M_{t_2}}{M_{t_1}}\right]^6 \left[\frac{C_2}{C_1}\right]^2 \left[\frac{r_1}{r_2}\right]^2 , \tag{6}$$

which is the conventional sixth power Mach number scaling law.

4. EXPERIMENTAL RESULTS AND DISCUSSION

4.1 Introduction

The effects of advance ratio, blade collective pitch, shaft angle, Mach number, and blade number on model helicopter rotor impulsive noise were studied. Blade slap contours were developed for presentation of the results of these experiments, as well as comparison with the baseline data. Blade slap windows detail the variations in C_T/σ for the operating conditions which exhibit blade slap. Although BVI blade slap for most operating conditions in this experiment results in one acoustic impulse per blade, a multiple impulse phenomenon was observed for certain specific conditions. Whereas the two and three-bladed blade slap contours were seen to be independent of tip speed, a comparison of the four-bladed configuration data obtained in Reference 2 with the present experimental results indicated some speed dependence of the contours.

The radiated sound was measured with a microphone located 48 inches directly below the rotor hub position at zero shaft tilt angle. For the conditions of these tests, this position was found to be the location of maximum blade slap intensity. Directivity studies of the blade slap at different tip speeds in two distinct orthogonal planes were done. Finally, a peak BVI blade slap Mach number scaling law developed for two-bladed rotors was applied to the three and four-bladed rotors to determine the accuracy of the law.

Although BVI impulsive noise has been documented as occuring on the retreating side of the rotor disc for a two-bladed rotor [20], for the conditions tested here for three and four-bladed rotors secondary (retreating side) blade slap was not detected.

4.2 Two-Bladed Rotor

Previous results obtained for a two-bladed rotor and contained in Reference 15 form the baseline for comparison of the parametric variations conducted in the present work. Figure 4.1 presents a blade slap contour for the two-bladed rotor. This contour indicates conditions which give rise to BVI blade slap. Although 327 ft/sec is the indicated rotational speed, the contour is independant of speed if advance ratio replaces tunnel speed as the abscissa, over the range of rotational speeds tested. Of primary importance in this figure is the shaded region identified as peak blade slap. Peak blade slap is defined as the maximum SPL obtained for a given shaft angle, and in general is usually located in the middle of the contour. It is this peak blade slap condition which is chosen for comparison with the Mach number scaling theory, for all blade number configurations. This baseline contour will be referred to often in the comparisons with the three and four bladed configurations.

Directivity patterns for the two-bladed rotor configuration had been acquired to aid in the identificaiton and quantification of the acoustic source mechanisms. These directivity measurements were made in a vertical plane normal to the tunnel wind axis as shown in Figure 2.1. These directivity patterns indicated the location of the maximum BVI blade slap intensity to be at the 90 degrees microphone location. The blade slap impulse was found to decrease in intensity until it was no longer detected at a microphone angle of 20 degrees.

An additional directivity pattern for the two-bladed rotor case was acquired. This directivity pattern of the BVI blade slap is in a vertical plane parallel with the tunnel wind axis, and normal to the original directivity plane. The 90 degree microphone position is common to both directivity patterns. The microphone is kept at a constant azimuthal angle (180 degrees), while the angle the radius vector makes with the horizontal varies from 90 degrees to 25 degrees. This corresponds to angles moving from directly below the rotor (90 degrees) to a position in the lower forward quadrant to the rotor (upstream).

Figure 4.2 presents the BVI blade slap acoustic time histories of this directivity pattern. Table 4.1 contains the SPLs for each of these time histories, along with the test conditions. The reader should be aware of scale changes in the acoustic pressure which make it possible to compare magnitudes of the blade slap only through use of the tabulated values. Also it is important to note that the 25 degrees microphone location is positioned within the tunnel stream. These microphone measurements were taken at a constant radial distance of 48 inches from the center of the rotor hub. A B&K Type UA0386 nose cone was used for all microphone locations, even though the other microphone positions were not judged to be in the tunnel stream.

As may be seen from the tabulated values, the peak blade slap intensity is also at 90 degrees for this directivity plane. The blade slap SPL decreases

until it is 4 dB down at 40 degrees. Although the 25 degree microphone location is down by 10 dB, it is felt that wind effects contribute significantly to this result. Although further tests should be conducted to quantify this effect of wind velocity, it is highly unlikely that it would account for the 7 dB drop associated with the move from 40 degrees to 25 degrees. The 25 degree location was chosen because the 30 degree position was partially obstructed by tunnel wall acoustic treatment.

The condition chosen for the directivity measurement of Table 4.1 corresponds to peak blade slap as determined by the 90 degrees microphone location. As one moves away from this peak blade slap advance ratio, the difference between SPLs at the different microphone locations is reduced. It was even positioned to obtain a weak BVI blade slap impulse at 40 degrees with no impulse evident at the 90 degrees location. In other words the directivity pattern appears to be a function of advance ratio. However it should be emphasized that the maximum dB level obtained during an advance ratio variation was from the 90 degree microphone location.

Table 4.2 provides SPLs for the original directivity pattern obtained in previous work [15]. Test conditions are nearly the same as those presented in Table 4.1. A comparison of these two directivity patterns shows the intensity of the BVI blade slap for the original directivity is more concentrated directly below the rotor than the new directivity pattern. We may say that the lobe is narrower for the original directivity pattern than the pattern in Table 4.1. This asymmetry may be related to the different dimensions of the blade in the spanwise and chordwise directions.

If we model the blade as a composite of a number of acoustically radiating elements in both the spanwise and chordwise direction, it may provide a possible explanation for the asymmetry of the directivity pattern. These elements are activated or excited as the pressure disturbance of the vortex moves outboard and downstream. The difference in dimensions of these two directions of this array of elements may be linked to the differences in directivity patterns, since array element number is known to be an important determining factor in acoustic radiation patterns.

This model of the BVI would represent the phenomenon as a non-compact or distributed group of acoustic dipoles. Also, the trailing edge of the blade becomes important, since the chord length determines one dimension of the array of elements. Both of these effects differ from the compact, point dipole model currently used for the BVI problem.

4.3 Three-Bladed Rotor

Figure 4.3 presents a blade slap contour acquired for a three-bladed rotor with θ_t = 2 degrees. This corresponds to a range of C_T/σ equivalent to that of the two-bladed configuration ($.070 \leq C_T/\sigma \leq .090$) contour shown in Figure 4.1. Once again it is noted that the shape of the contour itself is independent of the rotational speed over the range of Mach numbers tested. An obvious difference between the two and three-bladed rotor results is the range of shaft angles which give rise to BVI blade slap. The two-bladed results contain BVI blade slap for shaft angles up to -6 degrees. The three-bladed contour is limited to shaft angles of -4 degrees or less. One reason for this result is as follows. As shaft angle becomes more negative,

C_T/σ (blade loading) is reduced. This blade loading is directly related to the source strength of the BVI blade slap, which is a fluctuating lift mechanism. So, as we increase shaft angle, with other parameters constant, we reduce our BVI source strength. For the two-bladed configuration the source strength is strong enough to dominate the other noise sources (broadband and rotational) up to a -6 degree shaft angle. However, as we go to higher blade number, we increase the total blade surface area. This manifests itself as an increase in the broadband noise component present in the acoustic signal. The BVI blade slap source mechanism is no longer able to overcome the other noise components, and although BVI may still be taking place, blade slap is not present because the BVI acoustic impulse no longer dominates the acoustic time history. This is a limited explanation, since it does not take into account the more complicated issues of vortex position in the wake relative to the blades and spanwise interaction lengths and interaction angles of the blade/vortex encounter. These issues are beyond the scope of the present investigation, but are important.

Another difference in the contours is the effect of shaft angle on the blade slap boundary lines. The two-bladed rotor trends are more abrupt than the three-bladed rotor. The two-bladed configuration was found to contain three shaft angle regions of differing BVI blade slap behavior. The lower shaft angle regions ($|\alpha_s| \leq 2°$) was found to obey the Mach number to the sixth power (M_T^6) law. The high shaft angle region ($|\alpha_s| \leq 4°$) did not follow any consistent trends with M_T, although the BVI impulse were strong and steady. The transition region between the other two shaft angle regions was found to contain only an intermittent, greatly reduced BVI blade slap impulse. The three-bladed rotor does not contain this region of intermittent blade slap.

More importantly, however is the behavior of the BVI peak blade slap with respect to Mach number. For the three-bladed rotor, the peak blade slap SPLs show good agreement with the M_T^6 law for <u>all</u> shaft angles. Figure 4.4 presents these results. The scaling theory requires a reference SPL at a given speed to calculate resulting SPLs for other Mach numbers. All predicted values are based on peak SPLs acquired for ΩR = 262 ft/sec (1200 RPM).

No directivity patterns were acquired for the three-bladed configuration. The trends are similar to those determined for the two-bladed rotor and may be found in Reference 2.

Multiple BVI conditions were recorded. The additional impulse contained several characteristics. This impulse is separated by a constant distance in time from the intital blade slap impulse. The presence of this additional acoustic impulse causes an unsteadiness to appear in the initial impulse. These multiple phenomena occur at advance ratios below the peak blade slap advance ratio. This additioanl acoustic phenomenon may be associated with a blade interacting with more than one vortex in a revolution. The close spacing in time of the two impulse seems to preclude the possibility of one vortex interacting with more than one blade.

4.4 Four-Bladed Rotor

Tests conducted with the four-bladed rotor configuration consisted of θ_T variations at a constant shaft angle ($\alpha_s = 0°$). For this reason contours

similar to those obtained for two and three-bladed rotors are not presently available. However, important differnces in α_s = 0 degrees behavior between two and four-bladed configurations are indicated.

The previous two-bladed rotor studies found the advance ratio boundaries to be insensitive to changes in collective pitch (with shaft angle held constant). This is not the case for the four-bladed rotor. Table 4.3 shows the advance ratio boundaries as a function of collective pitch, θ_T. As θ_T is increased, the corresponding upper limit of advance ratio is increased. The lower limit of advance ratio changes only slightly, and this is also true of the advance ratio for peak blade slap. No comparison may be made with the three-bladed results, since θ_T was fixed for those experiments.

Figure 4.5 presents a comparison of the Mach number scaling theory with four-bladed rotor peak blade slap experimental results. Agreement is excellent, usually within 1 dB. The difference increases to about 1.5 dB at the higher speeds. Although this is still good agreement, this may indicate an effect which increases in importance at higher speeds.

Although no total directivity pattern was obtained, acoustic time histories and SPLs were acquired for the 40 degrees microphone location as presented in Figure 4.2. This was done for all peak blade slap conditions, and compared to the 90 degrees microphone data. At no time was the peak blade slap SPL at the 40 degrees microphone location found to be greater than the peak blade slap SPL at the 90 degrees location. The difference in SPLs was at least 4 dB and as much as 7 dB between the two microphone positions.

Finally, an additional speed effect on the blade slap boundaries was observed. A comparison of the four-bladed data of Reference 2 and the present results is given in Table 4.4. This table shows the advance ratio boundaries for various RPMs. Note that the upper limit of advance ratio for which blade slap exists increases monotonically. The last entry of this table represents data from the present experiments; all other data are from Reference 2. This indicated a strong dependence on tip speed of the upper limit of the blade slap boundaries. This was not the case for either the two or three-bladed rotors.

CONCLUSIONS AND RECOMMENDATIONS

A parametric study of model helicopter rotor blade slap has been conducted in the M.I.T. 5 by 7-1/2 ft. Anechoic Wind Tunnel Facility. Comparisons of 2, 3, and 4-bladed rotors have been made with respect to their BVI blade slap characteristics. A comparison with a Mach number scaling theory previously developed for prediction of peak blade slap SPL was conducted. The following conclusions may be drawn:

1) Three and four-bladed rotor configurations show very good agreement with the M_T^6 law for all conditions tested.
2) A reduction of conditions for which BVI blade slap may be detected was observed for three-bladed rotors, when compared to the two-bladed baseline.

3) The advance ratio boundaries of the four-bladed rotor exhibit a θ_T dependence not present for the two-bladed configuration.

4) The upper limits of the advance ratio boundaries of the four-bladed rotors increase with increasing rotational speed.

5) The BVI blade slap boundaries may be a function of microphone location.

6) Location of maximum BVI blade slap intensity is directly below the rotor.

7) An additional phenomenon is present in the acoustic traces of the three and four-bladed rotors. This consists of a one per blade impulse which closely follows the initial BVI impulse, and may be associated with an additional blade/vortex encounter.

Although this work reveals important similarities and differences in the nature of BVI blade slap as a function of blade number, a direct comparison of BVI blade slap intensity is not yet possible. Further investigations should be undertaken to provide a broader data base for three and four-bladed rotors as presently exists for two-bladed rotors. Especially useful and relevant would be $\theta_T(C_T/\sigma)$ variations for three-bladed rotors and shaft angle variations for four-bladed rotors.

Mach number scaling law comparisons should be conducted concurrently with the additional parametric variations suggested above. Also, the expanded Mach number capability of the new drive system should be exploited to determine the effects of increased speed on the accuracy of the M_T^6 law.

The use of analytical wake techniques together with flow visualization techniques may be employed to aid in a further understanding of the helicopter rotor aerodynamic environment which gives rise to the two per blade acoustic impulses. Also, the use of pressure transducers and hot-film gages on the surface of the blade would be valuable in discovering the characteristics of the fluid dynamics which account for the differences between blade number configurations noted here.

ACKNOWLEDGEMENTS

This research was supported in part by the NASA Langley Research Center under Grant No. NSG-1583.

REFERENCES

1) Chu, S. "An Unsteady Lifting Surface Theory for the Wing-Gust Interaction and its Application," Ph.D Thesis, M.I.T., 1975.

2) Hubbard, J. E., Jr., "A Parametric Study of Model Helicopter Blade Slap," Master of Science Thesis, M.I.T. 1978.

3) Crimi, P., "Prediction of Rotor Wake Flows," CAL/USAAVLABS Symposium Proceedings, Vol. 1, Propellor and Rotor Aerodynamics, Buffalo, N.Y., June 1966.

4) White, A. P., "VTOL Periodic Aerodynamic Loadings: The Problems, What is Being Done and What Needs to be Done," Journal of Sound and Vibration, Vol. 4, No. 3, pp. 282-394, 1966.

5) Tangler, J. L., "Schlieren and Noise Studies of Rotors in Forward Flight," Paper No. 77. 33-05, 33rd Annual National Forum of the American Helicopter Society, Washington, D.C., May 1977.

6) Hubbard, J. E., Jr., and Harris, W. L., "An Investigation of Model Helicopter Rotor Blade Slap at Low Tip Speeds," AIAA 5th Aeroacoustics Conference, Paper 79-0613, Seattle, Washington, March 1979.

7) Leighton, K. P., "A Parametric Study of Model Helicopter Rotor Blade Slap at Moderate Tip Speeds," Master of Science Thesis, M.I.T., 1981.

8) Charles, B. D., "Acoustic Effects of Rotor-Wake Interactions During Low Power Descent," presented at the National Symposium on Helicopter Aerodynamic Efficiency, Hartford, CT, March 1975.

9) Boxwell, D. A., and Schmitz, F. H., "Full-Scale Measurements of Blade-Vortex Interaction Noise," Paper 80-61, 36th Annual Forum of the American Helicopter Society, Washington, D.C., May 1980.

10) Schmitz, F. H., Boxwell, D. A., Lewy, S., and Dahan, C., "A Note on the General Scaling of Helicopter Blade-Vortex Interaction Noise." presented at the 38th Annual Forum of the American Helicopter Society, Anaheim, CA, 1982.

11) Hubbard, J. E., Jr. and Harris, W. L., "Model Helicopter Rotor Impulsive Noise," Journal of Sound and Vibration, 78 (3), 425-437, 1981.

12) Hoad, D. R., "Evaluation of Helicopter Noise Due to Blade-Vortex Interaction for Five Tip Configurations," NASA TP-1608, December 1979

13) Tangler, J. L., "The Design and Testing of a Tip to Reduce Blade Slap," Paper 963, 31st Annual National Forum of the American Helicopter Society, Washington, D.C., May 1986.

14) Leighton, K. P., Hubbard, J. E., Jr., Harris, W. L., and Peele, S. E. A., "Parametric Studies and Flow Visualization of Model Helicopter Rotor Blade Slap," AIAA 7th Aeroacoustics Conference, Paper 81-2002, Palo Alto, CA, October 1981.

15) Leighton, K. P., "Research on Model Helicopter Rotor Blade Slap at Moderate Tip Speeds," Journal of the American Helicopter Society, Vol. 27, No. 3, July 1982.

16) Hawkings, D. L., and Lowson, M. V., "Noise of High Speed Rotors, AIAA Paper No. 75-450, 2nd Aeroacoustics Conference, 1975.

17) Widnall, S. E., Harris, W. L., Lee, A. and Dress, H. M., "The Development of Experimental Techniques for the Study of Helicopter Rotor Noise," NASA CR-137684, 1974.

18) Harris, W. L., and Lee, A., "The Development of Experimental Techniques for the Study of Helicopter Rotor Noise," AIAA Paper 75-455, AIAA Second Aeroacoustics Conference, Hampton, VA, March 1975.

19) Lowson, M. V., and Ollerhead, J. B., "Studies of Helicopter Rotor Noise," USAAVLABS Technical Report 68-60, Wyle Laboratories, U. S. Army Aviation Material Laboratories, Fort Eustis, Virginia, 1969.

20) Aravamudan, K. S., Lee, A., and Harris, W. L., "A Simplified Mach Number Scaling Law for Helicopter Rotor Noise," Journal of Sound and Vibration, 57, (4) 555-570, 1978.

TABLE 2.1

MODEL ROTOR SPECIFICATIONS

Radius (R)	25 inches (63.6 cm)
Chord (C)	2 inches (5.08 cm)
Number of blades (B)	1 to 8
Section	NACA 0012
Twist	-8 degrees (linear)
Shaft tilt capability	+20 degrees, -10 degrees
Maximum RPM	3900
Testing RPM	Variable, from 0 to 2500
Lead-lag hinge	None
Cyclic pitch	None
Collective pitch	By manual adjustment of each blade
Hinge offset	1.5 inches (3.81 cm)

TABLE 4.1

TWO-BLADED DIRECTIVITY PATTERN

$\alpha_s = 0°$, $\mu = .17$; $C_T/\sigma = .105$; $\Omega R = 240$ ft/sec; $\theta_T = 5°$

Microphone Angle	SPL (dB re 20 μPa)
25°	96
40	103
50	104
60	105
70	105.5
80	106
90	107

TABLE 4.2

TWO-BLADED DIRECTIVITY PATTERN (Ref. 15)

$\alpha_s = 0°$, $\mu = .16$; $C_T/\sigma = .105$; $\Omega R = 240$ ft/sec; $\theta_T = 5°$

Microphone Angle	SPL (dB re 20 μPa)
30°	96
40	99
50	101
60	102
70	103
80	105
90	107

TABLE 4.3

FOUR-BLADED ROTOR BVI BLADE SLAP BOUNDARIES

μ_{LOW}	μ_{PEAK}	μ_{HIGH}	θ_T
.21	.23	.26	3°
.21	.24	.29	5°
.22	.24	.34	8°

TABLE 4.4

COMPARISION OF FOUR-BLADED ROTOR BLADE SLAP BOUNDARIES

RPM	μ	α_s
360-410	.26 - .23	0°
500-600	.27 - .22	0°
720-900	.28 - .22	0°
800-1000	.29 - .23	0°
1100	.34 - .22	0°

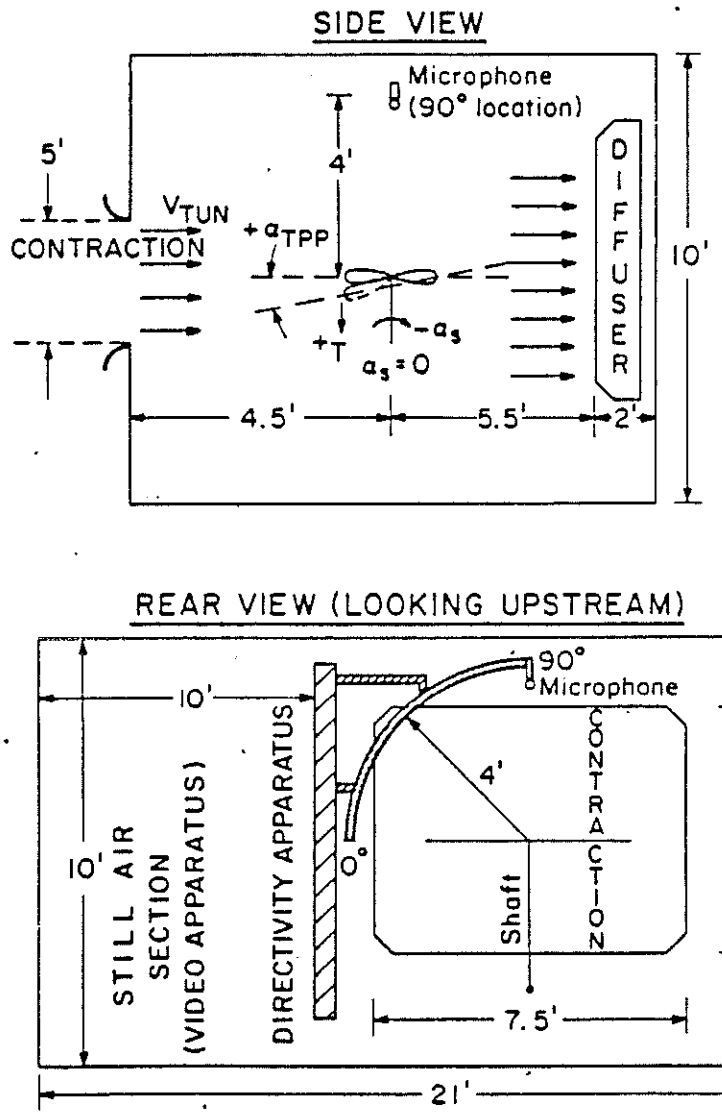

FIGURE 2.1 INVERTED ROTOR WIND TUNNEL CONFIGURATION

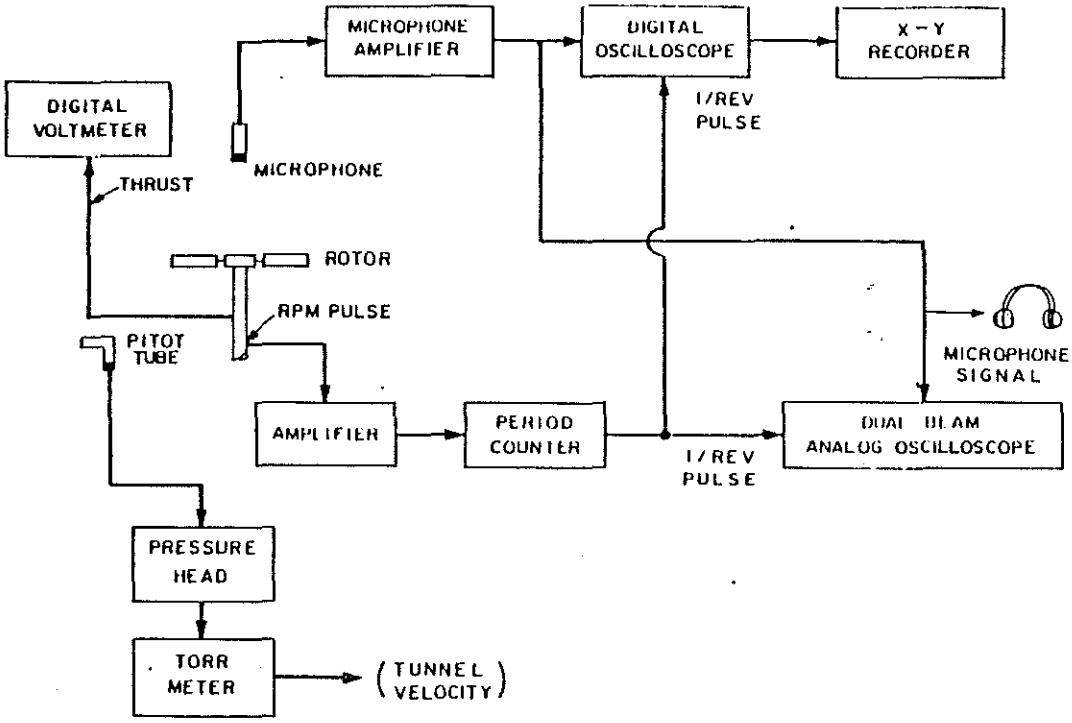

FIGURE 2.2 SCHEMATIC OF INSTRUMENTATION USED IN DATA ACQUISTION

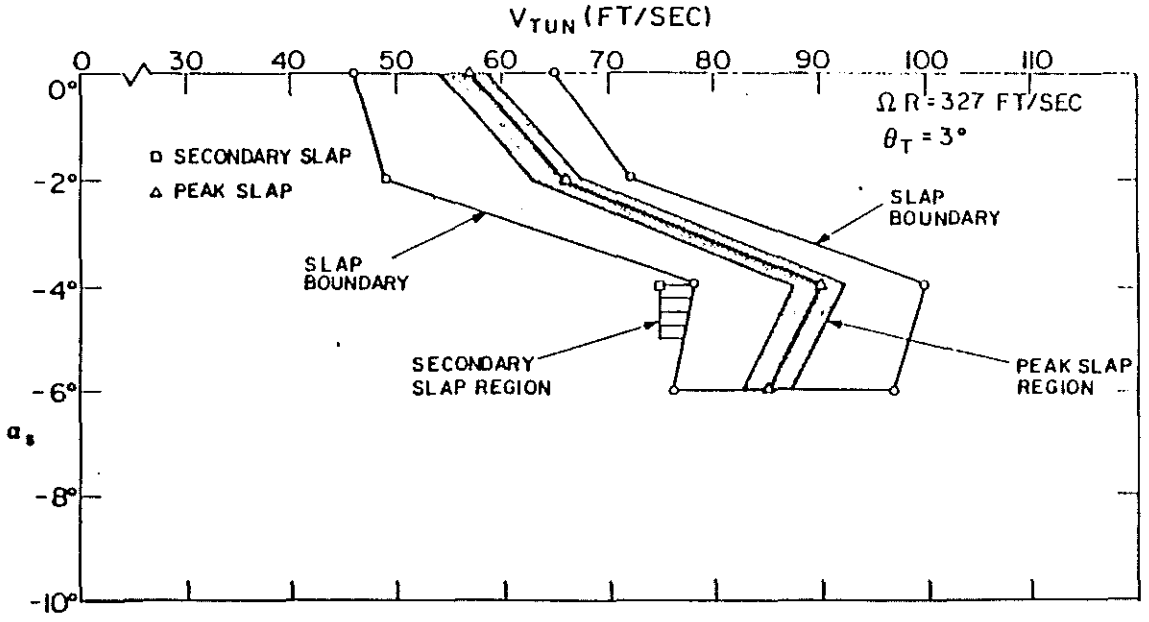

FIGURE 4.1 TWO-BLADED BVI SLAP CONTOUR

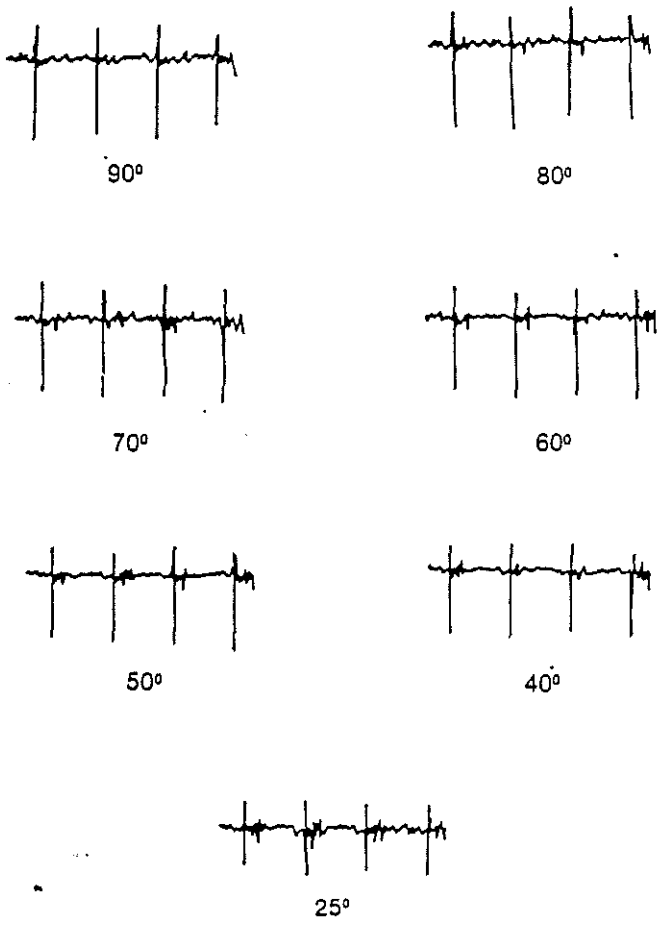

FIGURE 4.2 TWO-BLADED BVI DIRECTIVITY

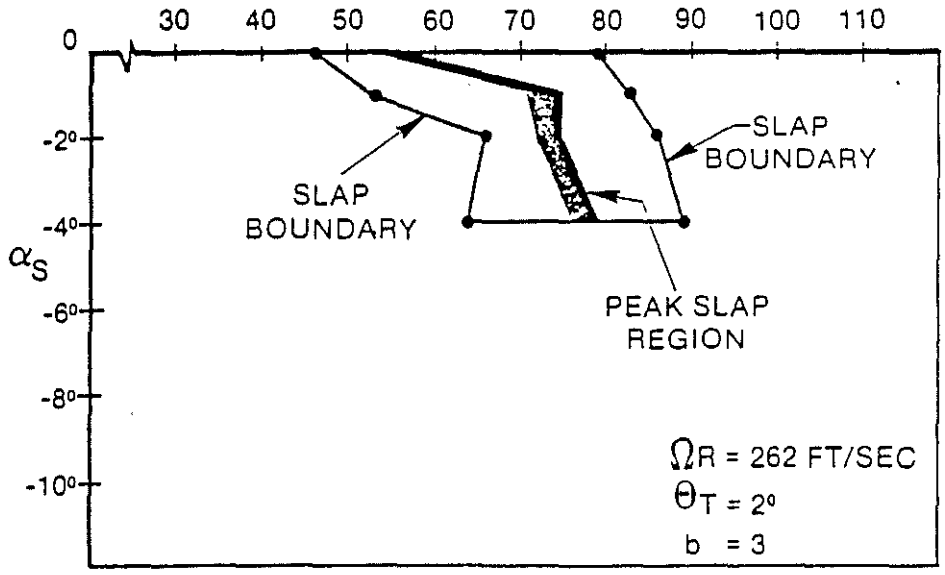

FIGURE 4.3 THREE-BLADED BVI CONTOUR

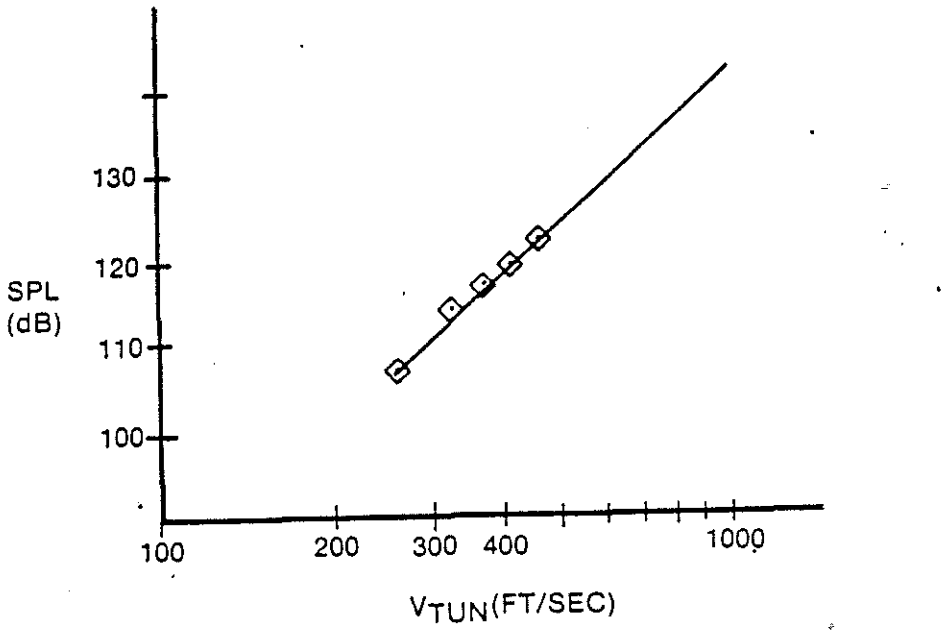

FIGURE 4.4 THREE-BLADED MACH NUMBER SCALING

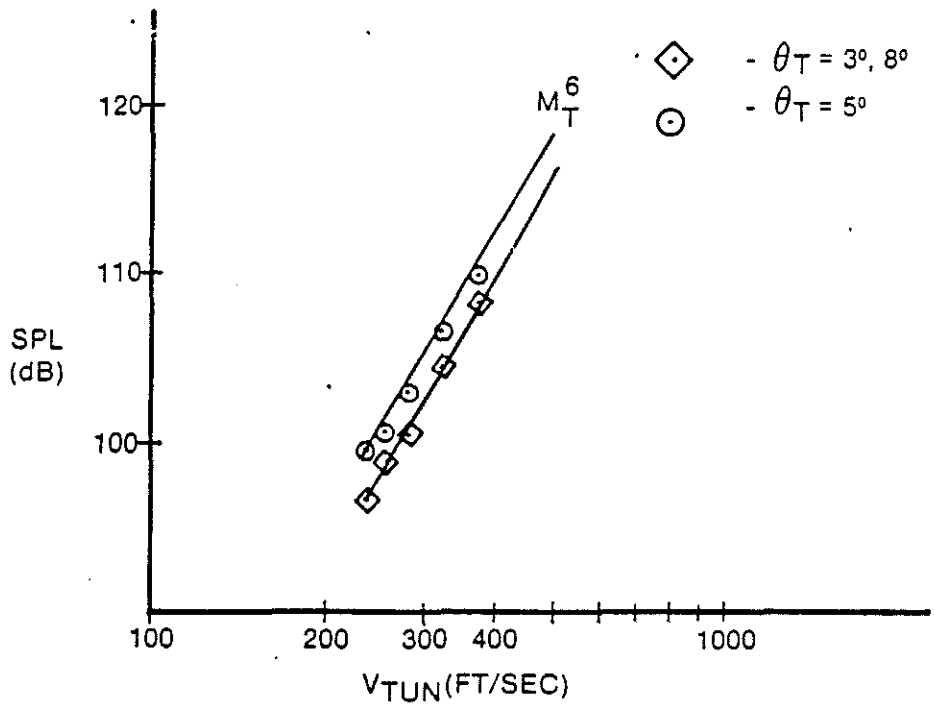

FIGURE 4.5 FOUR-BLADED MACH NUMBER SCALING